# $SrFe_2(PO_4)_2$: Ab Initio Structure Determination with X-ray Powder Diffraction Data and Unusual Magnetic Properties

Alexei A. Belik,*[,†,‡] Masaki Azuma,[†,‡] Mikio Takano,[†] and Bogdan I. Lazoryak[§]

*Institute for Chemical Research, Kyoto University, Uji, Kyoto-fu 611-0011, Japan, PRESTO, Japan Science and Technology Agency (JST), Kawaguchi, Saitama 332-0012, Japan, and Department of Chemistry, Moscow State University, Leninsky Gory, Moscow 119992, Russia*

*Received May 31, 2004. Revised Manuscript Received July 25, 2004*

Structure of $SrFe_2(PO_4)_2$ was solved ab initio from X-ray powder diffraction data (space group $P2_1/c$ (No. 14); $Z = 4$; $a = 9.3647(2)$ Å, $b = 6.8518(1)$ Å, $c = 10.5367(2)$ Å, and $\beta = 109.5140(8)°$). It has almost linear tetrameric units Fe2−Fe1−Fe1−Fe2 which join with each other through common oxygen atoms creating a complicated two-dimensional network parallel to the *bc* plane. Specific heat measurements revealed two phase transitions at $T_1 = 7.0$ K and $T_2 = 11.3$ K in zero magnetic field. The phase transition at $T_2$ seems to be a structural phase transition. Magnetization measurements showed that, below $T_1$, $SrFe_2(PO_4)_2$ exhibits weak ferromagnetism and demonstrates clear ferromagnetic hysteresis loops. Above 15 K, Curie−Weiss behavior was observed with an effective magnetic moment of 5.23 $\mu_B$ per $Fe^{2+}$ ion and Weiss constant of −18.9 K. Weak ferromagnetic properties below $T_1$ can be explained by canting of antiferromagnetically ordered spins. Several field-induced phase transitions were observed in $SrFe_2(PO_4)_2$ at low temperatures.

## 1. Introduction

Phosphates containing transition metals have been widely investigated because of the variety of their possible applications, e.g., as cathodes for Li batteries,[1] corrosion inhibitors,[2] heterogeneous catalysts,[3] and so forth, and diverse networks including porous ones. The complex structural chemistry of phosphates offers large variations of magnetic ion sublattices, which can give rise to original magnetic properties. Search for new structure types of phosphates is essential work for development of crystal chemistry of phosphates and their applications.

The structural variation of compounds with the nominal composition of $A^{2+}B^{2+}{}_2(PO_4)_2$ (A = Ca, Sr, Ba, and Pb; B = Mg and transition metals) is surprising. For example, the following compounds crystallize in different structure types: $CaCr_2(PO_4)_2$,[4] $SrMn_2(PO_4)_2$,[5] $SrCo_2(PO_4)_2$,[6] $SrNi_2(PO_4)_2$,[7] α-$SrZn_2(PO_4)_2$,[8] $BaCo_2(PO_4)_2$,[9] and $BaCu_2(PO_4)_2$.[10] Crystal structures as well as lattice parameters of $SrMg_2(PO_4)_2$,[11] β-$SrZn_2(PO_4)_2$,[11] and $SrCd_2(PO_4)_2$[12] are still unknown.

Two new compounds in this family, $SrFe_2(PO_4)_2$[13] and $SrCu_2(PO_4)_2$ (reported as $Sr_{1.9}Cu_{4.1}(PO_4)_4$ in ref 14), with unknown structures have recently been prepared and characterized. Second-harmonic generation (SHG) proved both compounds have centrosymmetric structures.[13,14] $SrCu_2(PO_4)_2$ demonstrated interesting magnetic properties, i.e., singlet ground state with a spin gap.[15] To understand these properties and correctly interpret them, the information about the structure is required. In ref 15, $SrCu_2(PO_4)_2$ was regarded as isotypic with $BaCu_2(PO_4)_2$ (space group $P\bar{1}$). Quite recently we could successfully determine the structure of $SrCu_2(PO_4)_2$ from X-ray powder diffraction (XRD) data and showed that $SrCu_2(PO_4)_2$ belongs to space group *Pccn* (No. 56) with $Z = 8$ and $a = 7.9422$ Å, $b = 15.3692$ Å, and $c = 10.3704$ Å.[16]

* To whom correspondence should be addressed. Telephone: +81-774-38-3122. FAX: +81-774-38-3125. E-mail: belik@msk.kuicr.kyoto-u.ac.jp.

† Kyoto University.

‡ JST.

§ Moscow State University.

(1) (a) Alvarez-Vega, M.; Garcia-Moreno, O.; Garcia-Alvardo, F.; Garcia-Jaca, J.; Gallardo-Amores, J. M.; Sanjuan, M. L.; Amador, U. *Chem. Mater.* **2001**, *13*, 1570. (b) Yang, S.; Zavalij, P. Y.; Whittingham, M. S. *Electrochem. Commun.* **2001**, *3*, 505.

(2) Bridson, J. N.; Quinlan, S. E.; Tremaine, P. R. *Chem. Mater.* **1998**, *10*, 763.

(3) (a) Millet, J.-M. M. *Catal. Rev.* **1998**, *40*, 1. (b) Bonnet, P.; Millet, J.-M. M.; Leclercq, C.; Vedrine, J. C. *J. Catal.* **1996**, *158*, 128.

(4) Maass, K.; Glaum, R.; Gruehn, R. *Z. Anorg. Allg. Chem.* **2002**, *628*, 1663.

(5) Elbali, B.; Boukhari, A.; Glaum, R.; Gerk, M.; Maass, K. *Z. Anorg. Allg. Chem.* **2000**, *626*, 2557.

(6) Elbali, B.; Boukhari, A.; Holt, E. M.; Aride, J. *J. Crystallogr. Spectosc. Res.* **1993**, *23*, 1001.

(7) Elbali, B.; Boukhari, A.; Aride, J.; Abraham, F. *J. Solid State Chem.* **1993**, *104*, 453.

(8) Hemon, A.; Courbion, G. *J. Solid State Chem.* **1990**, *85*, 164.

(9) Bircsak, Z.; Harrison, W. T. A. *Acta Crystallogr., Sect. C: Cryst. Struct. Commun.* **1998**, *54*, 1554.

(10) Moqine, A.; Boukhari, A.; Darriet, J. *J. Solid State Chem.* **1993**, *107*, 362.

(11) Sarver, J. F.; Hoffman, M. V.; Hummel, F. A. *J. Electrochem. Soc.* **1961**, *108*, 1103.

(12) Looney, J. R.; Brown, J. J. *J. Electrochem. Soc.* **1971**, *118*, 470.

(13) Belik, A. A.; Lazoryak, B. I.; Pokholok, K. V.; Terekhina, T. P.; Leonidov, I. A.; Mitberg, E. B.; Karelina, V. V.; Kellerman, D. G. *J. Solid State Chem.* **2001**, *162*, 113.

(14) Belik, A. A.; Malakho, A. P.; Lazoryak, B. I.; Khasanov, S. S. *J. Solid State Chem.* **2002**, *163*, 121.

(15) Mekata, M.; Hanabata, T.; Nakaya, K.; Ajiro, Y. *J. Magn. Magn. Mater.* **2001**, *226−230*, 410.

10.1021/cm049140o CCC: $27.50 
Published on Web 09/29/2004

$SrFe_2(PO_4)_2$ crystallizes in a monoclinic system.[13] It was characterized using Mössbauer and infrared spectroscopy at room temperature (RT), thermogravimetry in air, and magnetic susceptibility measurements above RT.[13]

In this paper, we describe the structure determination of $SrFe_2(PO_4)_2$ by direct methods from laboratory XRD data. We have investigated the magnetic properties of $SrFe_2(PO_4)_2$ by specific heat and direct current (dc) magnetization measurements. In zero magnetic field, $SrFe_2(PO_4)_2$ exhibits a structural phase transition at 11.3 K and a magnetic phase transition at 7.0 K to a weak ferromagnetic state due to spin canting. Temperature dependence of specific heat in $SrFe_2(PO_4)_2$ was strongly affected by static magnetic field. We have also observed several field-induced phase transitions at low temperatures.

## 2. Experimental Section

**Synthesis.** Single-phased $SrFe_2(PO_4)_2$ was synthesized from a mixture of $Sr_3(PO_4)_2$, $FePO_4$, and Fe (99.999%) with an amount-of-substance ratio of 1:4:2.[13] The mixture was contained in an alumina crucible and annealed under Ar at 1170−1190 K for 240 h with one intermediate grinding. The product was cooled with a furnace. $SrFe_2(PO_4)_2$ had white color. Single-phased $Sr_3(PO_4)_2$ and $FePO_4$ were prepared from mixtures of ($SrCO_3$ (99.999%) and $NH_4H_2PO_4$ (99.999%)) and ($Fe_2O_3$ (99.8%) and $NH_4H_2PO_4$), respectively, by the solid-state method at 1270 K for 100 h.

**XRD Procedures.** XRD data of $SrFe_2(PO_4)_2$ were measured at RT on a SIEMENS D500 Bragg−Brentano-type powder diffractometer operated at 30 kV and 30 mA. The diffractometer was equipped with an incident-beam quartz monochromator to obtain Cu $K\alpha_1$ radiation (wavelength, $\lambda = 1.5406$ Å) and a BRAUN position-sensitive detector. Si (NIST Standard Reference Material 640b) was used as an external standard material for diffraction angles ($2\theta$). XRD data were collected in a $2\theta$ range of 8−92° with a step width of 0.02°.

**Magnetic and Specific Heat Measurements.** dc magnetic susceptibility was measured on a Quantum Design SQUID magnetometer (MPMS XL) between 2 and 400 K in applied fields of 0.1, 5, 15, 30, and 50 kOe under both zero-field-cooled (ZFC) and field-cooled (FC) conditions. Isothermal magnetization curves were recorded between −50 and +50 kOe at 2, 5, 6, 7, 8, 9, 10, 11, 13, 15, and 110 K. dc magnetic susceptibility was also measured at 90 kOe under the FC condition from 50 to 2 K using a Quantum Design PPMS instrument. Specific heat, $C_p(T)$, was recorded between 2 and 60 K (on cooling) at zero magnetic field by a pulse relaxation method using a commercial calorimeter (Quantum Design PPMS). At magnetic fields of 0.1, 5, 10, 15, 30, 50, and 90 kOe, the $C_p(T)$ data were taken between 2 and 20 K (on heating). In these cases, the sample was cooled to 2 K at zero magnetic field and then the required magnetic field was applied.

## 3. Results and Discussion

**3.1. Crystal Structure.** For $SrFe_2(PO_4)_2$, a monoclinic cell with lattice parameters of $a \approx 9.36$ Å, $b \approx 6.85$ Å, $c \approx 10.54$ Å, and $\beta \approx 109.5°$ was given.[13] With these lattice parameters, reflection conditions derived from indexed reflections were $l = 2n$ for $h0l$ and $00l$ and $k = 2n$ for $0k0$, affording one centrosymmetric space group $P2_1/c$ (No. 14, unique axis $b$, cell choice 1),[17] in agreement with the results of SHG studies for $SrFe_2(PO_4)_2$.[13]

The structure of $SrFe_2(PO_4)_2$ was solved by direct methods with EXPO[18] using the default program's settings in space group $P2_1/c$ assuming $Z = 4$. With the EXTRA routine,[19] 238 independent reflections were extracted from the whole XRD pattern. A set of 13 independent atomic positions (one Sr, two Fe, two P, and eight O) was located from the E-map with the SIRPOW97 routine.[20]

Structure parameters were then refined by the Rietveld method with RIETAN-2000.[21] Coefficients for analytical approximation to atomic scattering factors for Sr, Fe, P, and O were taken from ref 22. The split pseudo-Voigt function of Toraya[23] was fit to each reflection profile, and a 10th-order Legendre polynomial was fit to the background. Isotropic atomic displacement parameters, $B$, with the isotropic Debye−Waller factor represented as $\exp((-B \sin^2\theta)/\lambda^2)$ were assigned to all of the sites. For oxygen atoms, $B$ parameters were fixed at 1 Å$^2$ and not refined.

Figure 1 shows experimental, calculated, and difference XRD patterns for $SrFe_2(PO_4)_2$. The final structure parameters are given in Table 1, and selected bond lengths, $l$, and angles, $\phi$, in Table 2. Figures 2−5 depict different fragments of the crystal structure.

The reasonable $l$(P−O), $l$(Fe−O), $l$(Sr−O), $B$(P), $B$(Fe), and $B$(Sr) values and sufficiently low $R$ factors indicate that the structure model for $SrFe_2(PO_4)_2$ is correct. In addition, the bond valence sum, $V$,[24] of each atom (Table 3) is in agreement with the formal oxidation state, also confirming the structure model.

Two independent positions of Fe atoms found in $SrFe_2(PO_4)_2$ are in agreement with Mössbauer spectroscopy data reported for $SrFe_2(PO_4)_2$.[13] The Mössbauer spectrum of $SrFe_2(PO_4)_2$ at RT was fitted by two doublets having approximately the same areas with isomer shifts, $\delta$, of 1.27 mm/s and quadrupole splitting, $\Delta E_Q$, of 2.60 and 2.93 mm/s.

The structure of $SrFe_2(PO_4)_2$ presents a new structure type among compounds with the nominal composition of $AB_2(XO_4)_2$ (A = Ca, Sr, Ba, and Pb; B = Mg and transition metals; X = P, V, and As). $Sr^{2+}$ ions in $SrFe_2(PO_4)_2$ are located at an 8-fold coordinated site. Two $SrO_8$ polyhedra are linked with each other by an edge (O6−O6), forming the $Sr_2O_{14}$ unit (Figure 2). $Fe^{2+}$ ions occupy two positions, Fe1 and Fe2, coordinated by six and seven O atoms, respectively (Figure 3). The polyhedron for Fe2 is better represented as $Fe2O_{5+2}$ because two distances, $l$(Fe2−O6) = 2.60 Å and $l$(Fe2−O1) = 2.69 Å, are rather long. However, the O1 and O6 atoms should be included in the coordination sphere of Fe2 because without these atoms $V$(Fe2) is too small (=1.621).

(16) Belik, A. A.; Azuma, M.; Takano, M. *International Conference on Magnetism*, Book of Abstracts, Roma, Italy, Jul 27−Aug 1, 2003; p 672.

(17) *International Tables for Crystallography*, Vol. A, 5th ed.; Hahn, T., Ed.; Kluwer: Dordrecht, The Netherlands, 2002; p 52.

(18) Altomare, A.; Burla, M. C.; Camalli, M.; Carrozzini, B.; Cascarano, G. L.; Giacovazzo, C.; Guagliardi, A.; Moliterni, A. G. G.; Polidori, G.; Rizzi, R. *J. Appl. Crystallogr.* **1999**, *32*, 339.

(19) Altomare, A.; Burla, M. C.; Cascarano, G.; Giacovazzo, C.; Guagliardi, A.; Moliterni, A. G. G.; Polidori, G. *J. Appl. Crystallogr.* **1995**, *28*, 842.

(20) Altomare, A.; Cascarano, G.; Giacovazzo, C.; Guagliardi, A.; Burla, M. C.; Polidori, G.; Camalli, M. *J. Appl. Crystallogr.* **1994**, *27*, 435.

(21) Izumi, F.; Ikeda, T. *Mater. Sci. Forum* **2000**, *321−324*, 198.

(22) *International Tables for Crystallography*, Vol. C, 2nd ed.; Wilson, A. J. C., Prince, E., Eds.; Kluwer: Dordrecht, The Netherlands, 1999; pp 572−574.

(23) Toraya, H. *J. Appl. Crystallogr.* **1990**, *23*, 485.

(24) Brown, I. D.; Altermatt, D. *Acta Crystallogr., Sect. B: Struct. Sci.* **1985**, *41*, 244.

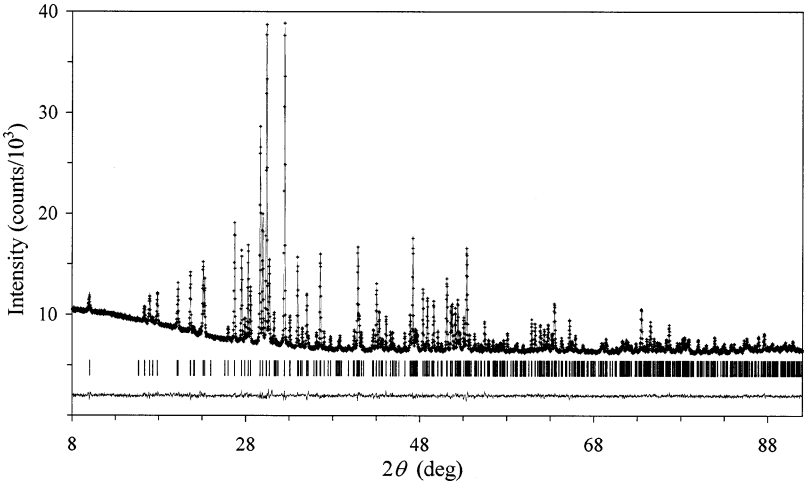


**Figure 1.** Observed (crosses), calculated (solid line), and difference XRD patterns for $SrFe_2(PO_4)_2$. Bragg reflections are indicated by tick mark.

**Table 1. Fractional Coordinates and Isotropic Atomic Displacement Parameters for $SrFe_2(PO_4)_2$[a]**

| site[b] | $x$ | $y$ | $z$ | $B$ (Å$^2$) |
|---|---|---|---|---|
| Sr | 0.3041(2) | 0.1224(3) | 0.0162(2) | 0.61(5) |
| Fe1 | 0.0829(3) | 0.6514(4) | 0.1184(2) | 0.95(7) |
| Fe2 | 0.2879(3) | 0.8942(4) | 0.3376(2) | 0.83(8) |
| P1 | 0.0363(4) | 0.1729(6) | 0.1693(4) | 0.06(10) |
| P2 | 0.4267(5) | 0.8547(7) | 0.6237(4) | 0.55(10) |
| O1 | 0.1067(11) | 0.2055(12) | 0.3202(9) | 1.0[c] |
| O2 | 0.1128(10) | −0.0082(12) | 0.1369(7) | 1.0[c] |
| O3 | 0.1391(9) | 0.6513(13) | 0.3629(7) | 1.0[c] |
| O4 | 0.0675(10) | 0.3425(13) | 0.0824(8) | 1.0[c] |
| O5 | 0.4249(9) | 0.0883(13) | 0.2691(9) | 1.0[c] |
| O6 | 0.4504(10) | 0.6838(13) | 0.5396(9) | 1.0[c] |
| O7 | 0.3414(9) | 0.0224(11) | 0.5198(9) | 1.0[c] |
| O8 | 0.3083(10) | 0.6910(11) | 0.1921(8) | 1.0[c] |

[a] Space group $P2_1/c$ (No. 14, cell choice 1); $a$ = 9.3647(2) Å, $b$ = 6.8518(1) Å, $c$ = 10.5367(2) Å, and $\beta$ = 109.5140(8)°; $Z$ = 4; $R_{wp}$ = 1.46%, $R_p$ = 1.14%, $R_B$ = 2.02%, $R_F$ = 1.65%, and $S = R_{wp}/R_e$ = 1.29. [b] The occupancies of all the sites are 1. The Wyckoff notation of all the sites is 4*e*. [c] Fixed values.

**Table 2. Bond Lengths, $l$, and Angles, $\phi$, in $SrFe_2(PO_4)_2$**

| bonds | $l$ (Å) | bonds | $l$ (Å) |
|---|---|---|---|
| Sr−O7 | 2.457(8) | Fe2−O7 | 2.016(8) |
| Sr−O6 | 2.472(9) | Fe2−O8 | 2.127(8) |
| Sr−O5 | 2.535(9) | Fe2−O5 | 2.134(8) |
| Sr−O1 | 2.554(9) | Fe2−O3 | 2.243(9) |
| Sr−O6 | 2.590(9) | Fe2−O2 | 2.300(8) |
| Sr−O3 | 2.616(8) | Fe2−O6 | 2.601(9) |
| Sr−O2 | 2.675(8) | Fe2−O1 | 2.693(8) |
| Sr−O4 | 2.951(9) | | |
| Sr−O8 | 3.482(9) | | |
| Fe1−O8 | 2.009(9) | P1−O1 | 1.520(8) |
| Fe1−O4 | 2.114(8) | P1−O2 | 1.527(8) |
| Fe1−O1 | 2.116(11) | P1−O4 | 1.566(9) |
| Fe1−O4 | 2.147(9) | P1−O3 | 1.570(8) |
| Fe1−O2 | 2.350(9) | P2−O5 | 1.520(8) |
| Fe1−O3 | 2.451(7) | P2−O6 | 1.529(9) |
| Fe1−O7 | 3.167(9) | P2−O8 | 1.543(9) |
| Fe1−O3 | 3.210(7) | P2−O7 | 1.604(8) |
| **angles** | **$\phi$ (deg)** | **angles** | **$\phi$ (deg)** |
| O1−P1−O2 | 106.3(5) | O5−P2−O6 | 110.7(6) |
| O1−P1−O3 | 107.3(6) | O5−P2−O7 | 116.5(5) |
| O1−P1−O4 | 113.7(6) | O5−P2−O8 | 109.1(5) |
| O2−P1−O3 | 114.2(5) | O6−P2−O7 | 106.8(5) |
| O2−P1−O4 | 106.2(5) | O6−P2−O8 | 112.4(5) |
| O3−P1−O4 | 109.3(5) | O7−P2−O8 | 101.1(5) |

The $Fe1O_6$ polyhedron also has two longer distances, $l$(Fe1−O2) = 2.35 Å and $l$(Fe1−O3) = 2.45 Å, in comparison with other $l$(Fe1−O) ≤ 2.15 Å.

Two $Fe1O_6$ polyhedra have a common edge (O4−O4) forming the $Fe1_2O_{10}$ unit. One $Fe1_2O_{10}$ unit and two $Fe2O_7$ polyhedra are connected with each other by two faces (O2−O3−O8) in such a way that they create almost linear tetrametic unit Fe2−Fe1−Fe1−Fe2 with $l$(Fe1−Fe2) = 2.97 Å and $l$(Fe1−Fe1) = 3.22 Å (Figure 4). The Fe−Fe distances with the neighboring Fe2−Fe1−Fe1−Fe2 units are $l$(Fe1−Fe2) = 4.04 Å, and $l$(Fe1−Fe2) = 4.06 Å. The Fe2−Fe1−Fe1−Fe2 units are linked with each other by corners (O1), creating a complicated two-dimensional network parallel to the *bc* plane (Figure 5). The $Sr_2O_{14}$ units and $P1O_4$ and $P2O_4$ tetrahedra join the planes formed by $Fe1_2O_{10}$ and $Fe2O_7$ (Figure 3). Note that despite the comparable Fe1−Fe2 distances between neighboring tetramers, they are connected only through the O1 atom because the Fe1−O7 distance is too long (3.167 Å).

It is interesting to compare the structure of $SrFe_2(PO_4)_2$ with those of $SrB_2(PO_4)_2$ (B = Mn,[5] Co,[6] Ni,[7] Cu,[16] and Zn[8]). In all these compounds, $SrO_n$ polyhedra have connections with each other by edges. In $SrNi_2(PO_4)_2$, $SrO_8$ polyhedra linked by two edges form infinite single chains. In $SrCo_2(PO_4)_2$ and $SrMn_2(PO_4)_2$, $Sr_2O_{2n-2}$ units are joined by corners forming double chains. $Sr_2O_{2n-2}$ units are isolated from each other in $SrFe_2(PO_4)_2$, $SrCu_2(PO_4)_2$, and $SrZn_2(PO_4)_2$. $Zn1O_4$ and $Zn2O_4$ tetrahedra have no connections with each other in $SrZn_2(PO_4)_2$, while $Co1O_{4+1}$ and $Co2O_4$ polyhedra form tetrameric units in $SrCo_2(PO_4)_2$. In $SrNi_2(PO_4)_2$, there are $Ni1_2O_{10}$ and $Ni2_2O_{10}$ units which are linked with each other by corners to create planes. $Mn1O_6$, $Mn2O_{5+1}$, $Mn3O_{5+1}$, and $Mn4O_5$ polyhedra in $SrMn_2(PO_4)_2$ have common edges and corners, also forming planes. $Cu1O_{4+1}$ and $Cu2O_{4+1}$ polyhedra are connected by an edge and create the dimer unit $Cu_2O_8$ in $SrCu_2(PO_4)_2$. Thus, the structure of $SrFe_2(PO_4)_2$ has unique connections of $Sr_2O_{14}$ and $Fe1_2O_{10}$ units and $Fe2O_7$ polyhedra with each other.

**3.2. Magnetic Properties.** Figure 6a shows temperature dependence of $C_p$ and $C_p/T$ at zero magnetic field. Two peaks were clearly seen on these curves at $T_1$ = 7.0 K and $T_2$ = 11.3 K. It is very difficult to estimate the lattice contribution from these data. Magnetic specific heat cannot, therefore, be evaluated. The peak

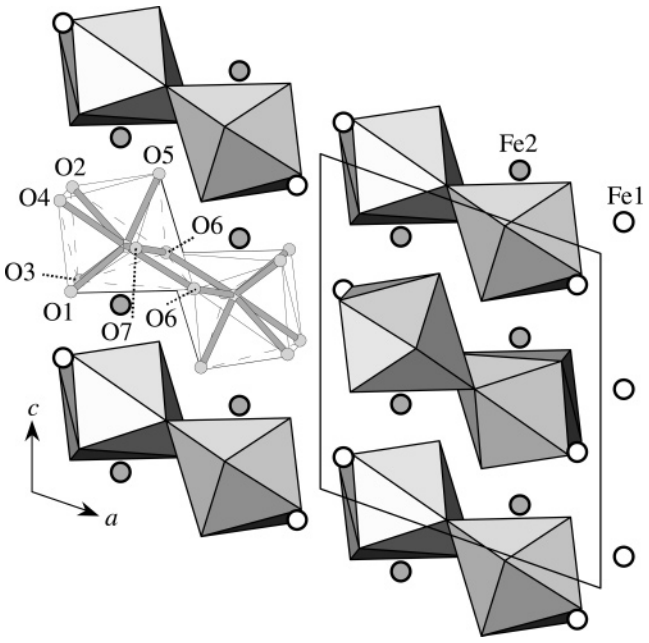


**Figure 2.** Projection of the structure of $SrFe_2(PO_4)_2$ along the *b* axis. $Sr_2O_{14}$ units are shown. Fe1 and Fe2 atoms are presented by circles. For one $Sr_2O_{14}$ unit, the Sr−O bonds are given by balls and sticks. $PO_4$ tetrahedra are omitted.

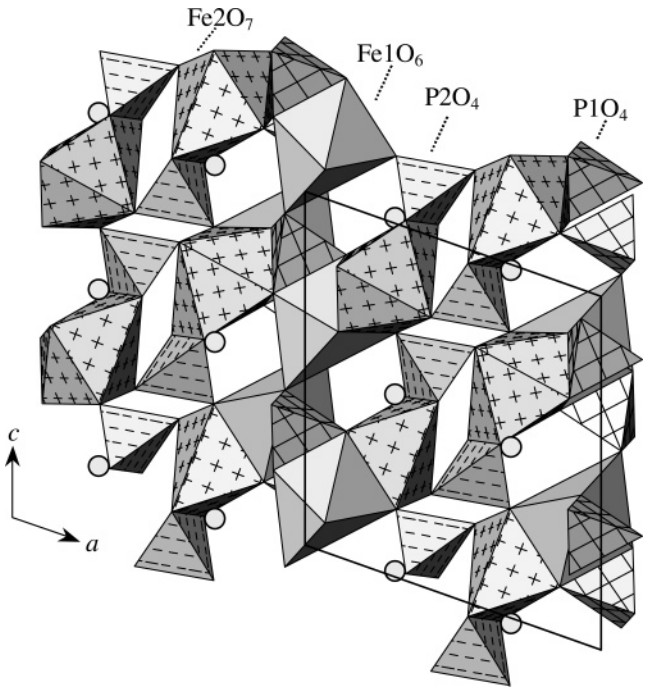


**Figure 3.** Projection of the structure of $SrFe_2(PO_4)_2$ along the *b* axis. $Fe1O_6$ and $Fe2O_7$ polyhedra and $PO_4$ tetrahedra are shown. Sr atoms are given by circles.

at $T_1$ was rather narrow and the $C_p/T$ values started to decrease sharply below $T_1$. On the other hand, the peak at $T_2$ was much broader than that at $T_1$.

The $C_p/T$ vs $T$ curves at different magnetic fields are presented in Figure 6b. No change of the intensity of the peak at $T_2$ and its position was seen below and at 15 kOe. However the first peak corresponding to $T_1$ became much broader and its maximum shifted to higher temperatures with increasing magnetic field. The area of the first peak in magnetic fields was much larger than that in zero magnetic field.

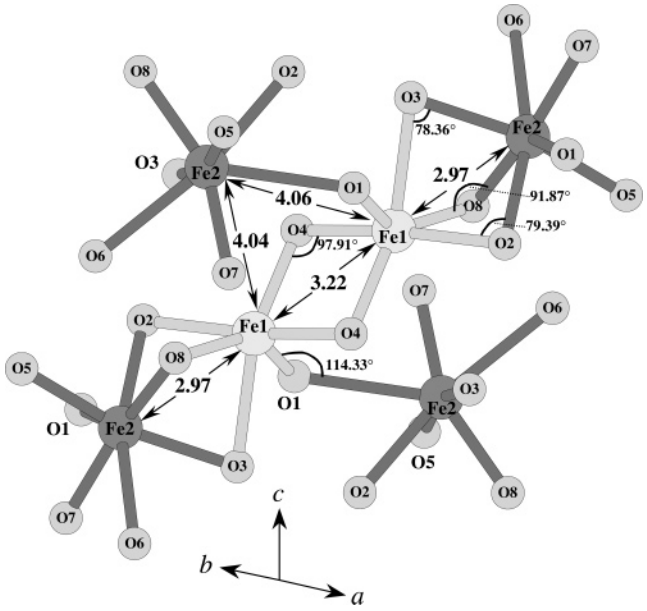


**Figure 4.** $Fe1_2O_{10}$ unit and $Fe2O_7$ polyhedra in the structure of $SrFe_2(PO_4)_2$. Interatomic distances (Å) and bond angles are given.

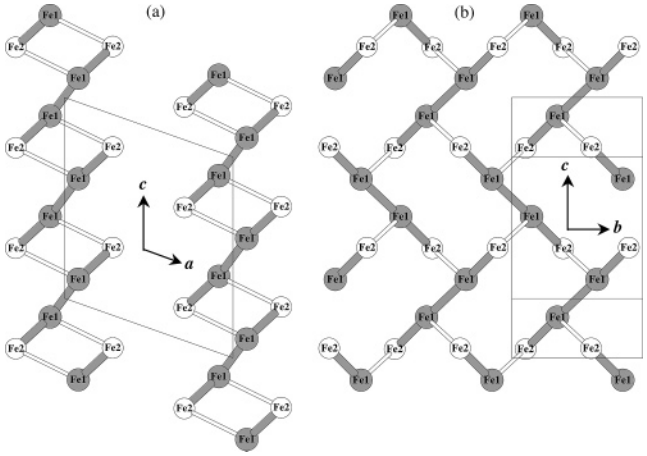


**Figure 5.** Layers formed by the Fe1 and Fe2 atoms in the structure of $SrFe_2(PO_4)_2$. (a) Projections of two layers along the *b* axis. (b) Projection of one layer on the *bc* plane. The thick bonds present the connections inside the tetramer Fe2−Fe1−Fe1−Fe2 units. The thin bonds show the connections between the tetramer units (through the O1 atoms).

**Table 3. Bond Valence Sum, *V*, in $SrFe_2(PO_4)_2$**

| atom | O1 | O2 | O3 | O4 | O5 | O6 | O7 | O8 | *V* |
|---|---|---|---|---|---|---|---|---|---|
| Sr | 0.308 | 0.222 | 0.260 | 0.105 | 0.324 | 0.279<br>0.384 | 0.400 | | 2.282 |
| Fe1 | 0.357 | 0.190 | 0.144 | 0.329<br>0.359 | | | | 0.477 | 1.856 |
| Fe2 | 0.075 | 0.217 | 0.253 | | 0.339 | 0.096 | 0.466 | 0.346 | 1.792 |
| P1 | 1.299 | 1.274 | 1.136 | 1.148 | | | | | 4.857 |
| P2 | | | | | 1.300 | 1.268 | 1.037 | 1.222 | 4.827 |
| *V* | 2.039 | 1.903 | 1.793 | 1.941 | 1.963 | 2.027 | 1.903 | 2.045 | |

A new feature appeared on the $C_p/T$ vs $T$ curves at higher magnetic fields (at 30 and 50 kOe), i.e., the peak with a maximum near $T_3$ = 12.3 K. The first peak continued to become more diffuse with increasing magnetic field, and its maximum shifted to the higher temperatures. The $C_p/T$ vs $T$ dependence changed again at 90 kOe. The curve at 90 kOe was close to that at 50 kOe except for the peak at 12.3 K. Note that, at 30 kOe

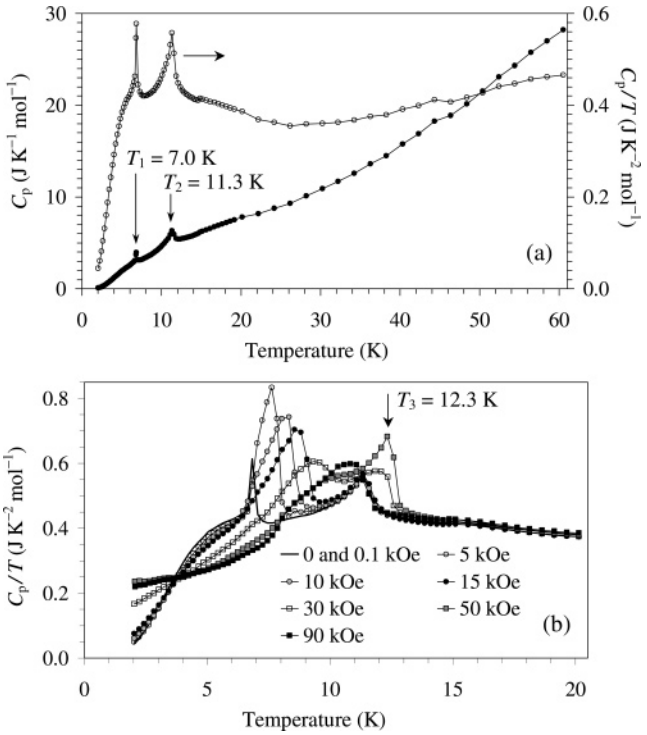


**Figure 6.** (a) Temperature dependence of specific heat, $C_p$, and $C_p/T$ for $SrFe_2(PO_4)_2$ at zero magnetic field between 2 and 60 K. (b) $C_p/T$ versus $T$ curves at 0, 0.1, 5, 10, 15, 30, 50, and 90 kOe in the temperature range of 2−20 K.

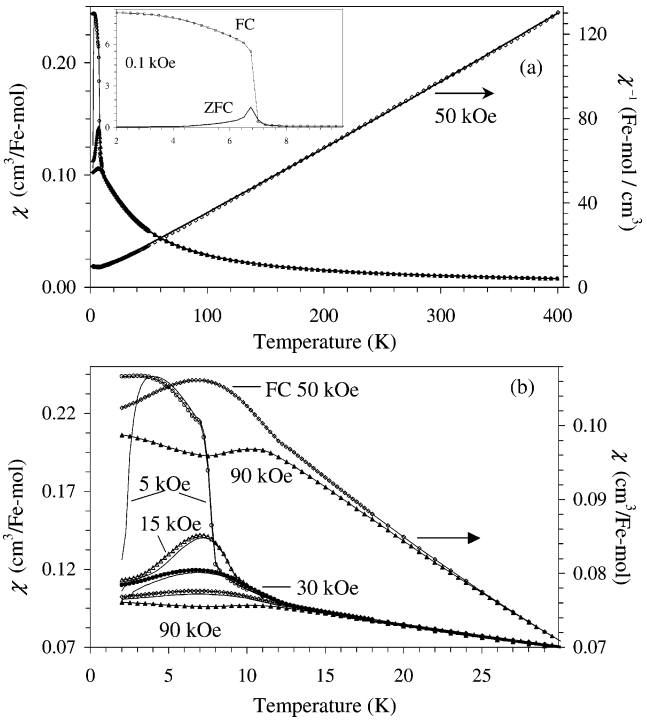


**Figure 7.** (a) Magnetic susceptibilities, $\chi$, against temperature, $T$, for $SrFe_2(PO_4)_2$ at 5 (circles), 15 (triangles), and 50 (diamonds) kOe and the FC $\chi^{-1}(T)$ curve at 50 kOe (diamond symbols) with the Curie−Weiss fit (solid line). ZFC (thin lines) and FC (lines with symbols) curves are shown for $\chi(T)$. Inset shows the ZFC and FC $\chi(T)$ curves at 0.1 kOe between 2 and 9.8 K. (b) The enlarged fragment of panel a with the $\chi(T)$ curves at 5, 15, 30 (black circles), 50, and 90 (black triangles) kOe. The FC curves at 50 and 90 kOe are also drawn using the secondary $y$ axis.

and higher magnetic fields, no distinct maximum was observed at $T_2$ because of overlapping with other anomalies.

At fields above and at 30 kOe, the $C_p/T$ vs $T$ curves in the low-temperature region (below 6.5 K) changed their behavior in comparison with the curves measured below and at 15 kOe. Above 14 K, actually no field dependence of the $C_p/T$ vs $T$ curves was observed.

From the specific heat data, at least two phase transitions induced by high magnetic fields were detected in $SrFe_2(PO_4)_2$. One of them is between 15 and 30 kOe, and another one is between 50 and 90 kOe.

Figure 7 depicts dc magnetic susceptibility ($\chi = M/H$) versus temperature curves at 0.1, 5, 15, 30, 50, and 90 kOe. Above ~15 K, no noticeable difference was found between the ZFC and FC curves and between the curves measured at different magnetic fields. The $\chi^{-1}(T)$ data (measured at 50 kOe) at 15−400 K were fitted by a modified Curie−Weiss expression, $\chi(T) = \chi_0 + C/(T - \theta)$, with temperature-independent term $\chi_0 = -4.6(4) \times 10^{-4}$ cm$^3$/Fe-mol, Curie constant $C = 3.416(16)$ cm$^3$ K/Fe-mol, and Weiss constant $\theta = -18.9(4)$ K (Figure 7a). The effective magnetic moment ($\mu_{eff} = (8C)^{1/2}$) was calculated to be 5.23 $\mu_B$ per $Fe^{2+}$ ion. This value is typical for high-spin $Fe^{2+}$ ions. The negative Weiss constant implies antiferromagnetic interactions between $Fe^{2+}$ ions.

Below ~12 K, deviation from the Curie−Weiss behavior on the $\chi(T)$ curves started. At magnetic fields of 0.1 and 5 kOe, the large difference between the ZFC and FC curves was observed. The FC curves increased rapidly below ~7 K ($T_1$) and then reached constant values at the lowest temperatures. The $d(\chi T)/dT$ vs $T$ curves (Figure 8) showed a sharp peak with a negative gradient at $T_1$ characteristic of weak ferromagnets.

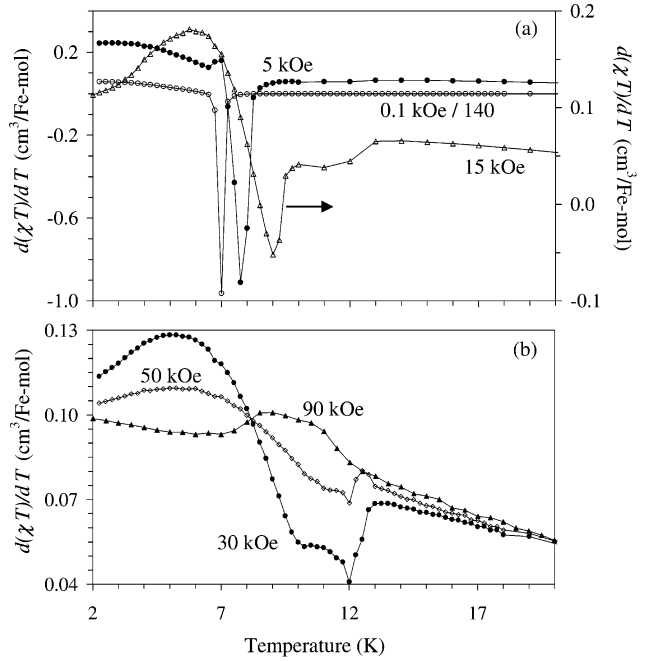


**Figure 8.** Details of the $d(\chi T)/dT$ vs $T$ curves in the FC mode at (a) 0.1, 5, and 15 kOe and (b) 30, 50, and 90 kOe in the temperature range of 2−20 K.

Different behavior of the $\chi(T)$ curves was detected in magnetic fields of 15, 30, and 50 kOe. In these cases, the ZFC and FC curves were close to each other in shape but slightly differed from each other in values below ~12

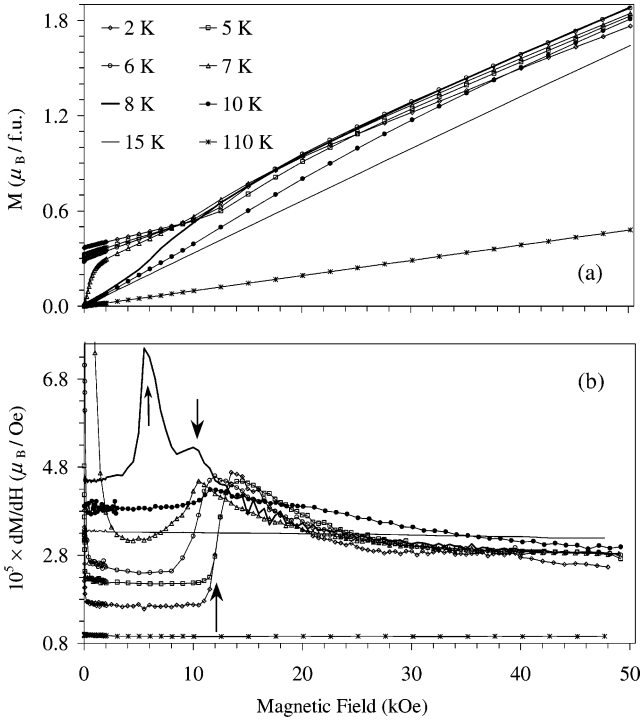


**Figure 9.** (a) Isothermal magnetization curves ($M$ vs $H$) at 2, 5, 6, 7, 8, 10, 15, and 110 K. The present curves were measured from 50 kOe to 0 Oe. (b) d$M$/d$H$ vs $H$ curves at the same temperatures. Arrows indicate anomalies on these curves.

K. The FC curves showed humplike behavior below 12 K. The FC data decreased with decreasing temperature below the hump. At 30 and 50 kOe, no peaks were found at $T_1$ on the d($\chi T$)/d$T$ vs $T$ curves but only a broad anomaly near 10 K and a small sharp anomaly near ~12 K ($T_3$) with negative gradient were detected (Figure 8b) in accordance with the $C_p(T)$ data.

The $\chi(T)$ (Figure 7b) and d($\chi T$)/d$T$ vs $T$ (Figure 8b) curves at 90 kOe differed from those measured at 30 and 50 kOe. At 90 kOe, the broad maximum on the FC $\chi(T)$ curve was centered at ~10.5 K, but the $\chi$ values started to increase again with decreasing temperature from ~8 to 2 K. The d($\chi T$)/d$T$ vs $T$ curve at 90 kOe showed no anomalies with negative gradient.

Thus, the $\chi(T)$ and d($\chi T$)/d$T$ vs $T$ data indicated the presence of two field-induced transformations; the first one is between 5 and 15 kOe, and the second one is between 50 and 90 kOe.

Additional insight into the low-temperature magnetic states can be obtained by recording isothermal magnetization curves (Figures 9−11). Above $T_3$ (at 13, 15, and 110 K), only the anticipated linear paramagnetic response and no hysteresis loop were detected on the M vs H curves (Figure 9a). The d$M$/d$H$ vs $H$ curves also showed no anomaly at 13, 15, and 110 K (Figure 9b). Between $T_1$ and $T_3$ (at 8, 9, 10 and 11 K), the magnetization curves passed through the origin and they changed their slope at characteristic fields. For example at 8 K, the d$M$/d$H$ vs $H$ curve showed two peaks at about 6 and 10 kOe. From 0 to 6 kOe at 8 K, we observed a linear behavior anticipated for a paramagnetic state. Above this field, the curve slope changed (Figure 9b) that corresponds to the situation when the first peak on the $C_p/T$ vs $T$ curves started to cross the temperature of 8 K (Figure 6b).

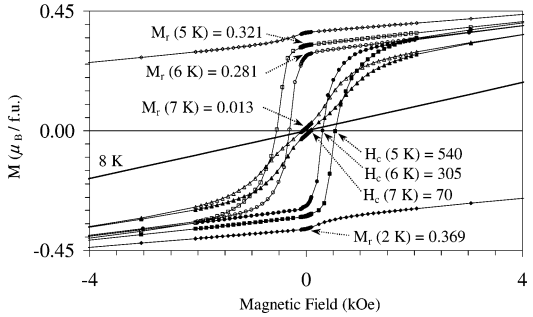


**Figure 10.** $M$ vs $H$ curves at 2, 5, 6, 7, and 8 K in the magnetic field strength range of −4 to +4 kOe. Remanent moments, $M_r$ ($\mu_B$/fu), and coercitive fields, $H_c$ (Oe), are given in the figure. f.u.: formula unit.

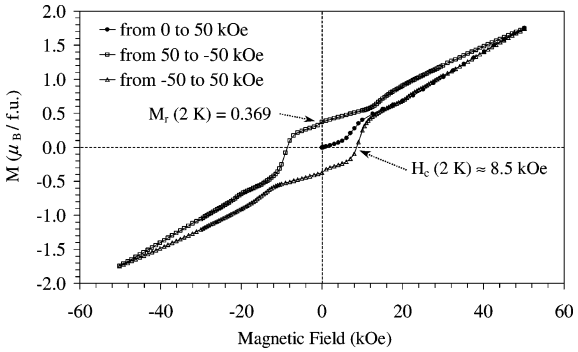


**Figure 11.** $M$ vs $H$ curves at 2 K in the magnetic field strength range from −50 to +50 kOe. The values of $M_r$ and $H_c$ are given in the figure.

**Table 4. Estimated Values of the Saturated Weak Ferromagnetic Moments ($M_0$), Induced Ferromagnetic Moments ($M_I$), Remanent Moments ($M_r$), and Coercitive Fields ($H_c$) for $SrFe_2(PO_4)_2$**

| $T$ (K) | $M_0$ ($\mu_B$/fu)[a] | $M_I$ ($\mu_B$/fu)[b] | $M_r$ ($\mu_B$/fu) | $H_c$ (Oe) |
|---|---|---|---|---|
| 2 | 0.371 | 0.406 | 0.369 | ~8500 |
| 5 | 0.325 | 0.369 | 0.321 | 540 |
| 6 | 0.296 | 0.406 | 0.281 | 305 |
| 7 | 0.229 | 0.407 | 0.013 | 70 |
| 8 | | 0.387 | | |
| 9 | | 0.321 | | |
| 10 | | 0.229 | | |
| 11 | | 0.154 | | |

[a] The $M_0$ values were estimated by linear extrapolation between 2 and 10 kOe to $H = 0$ Oe. [b] The $M_I$ values were estimated by linear extrapolation between 30 and 50 kOe to $H = 0$ Oe.[29]

Below $T_1$ (at 2, 5, and 6 K), the clear ferromagnetic hysteresis loop (the first hysteresis) was recorded (Figures 10 and 11). Once the saturation of the weak ferromagnetic moment has been reached, the magnetization curves followed the straight line $M = M_0 + \chi H$ (where $M_0$ is the saturated weak ferromagnetic moment and $\chi$ is the susceptibility of the antiferromagentic state) but only up to about 10−12 kOe. The values of $M_0$, remanent moments ($M_r$), and coercitive fields ($H_c$) are listed in Table 4. Above 10−12 kOe, the $M$ *vs* $H$ curves measured below $T_1$ changed their slope and resembled those measured between $T_1$ and $T_3$ as shown in Figure 9. Thus, the $M$ vs $H$ and d$M$/d$H$ vs $H$ data confirmed the presence of two magnetic regimes above and below 10−12 kOe as suggested from the $\chi(T)$ data.

At 5 and 6 K, a small hysteresis on the $M$ vs $H$ curves was also observed between ~10 and ~50 kOe (the second hysteresis), whereas a very small hysteresis was

found between ~5 and ~20 kOe at 8 K. The second hysteresis was rather noticeable at 2 K (Figure 11). Striking differences were observed in the isothermal behavior of the $M$ vs $H$ curves at 2 K compared to those at 5 and 6 K. Although it is common for the coercitive field and the remanent moment to increase with decreasing temperature, the strong increase of the coercitive field between 2 and 5 K is remarkable. This behavior can be explained by an increase of the magnetic anisotropy of $Fe^{2+}$ ions as the temperature decreased from 5 K.[25]

The peak at $T_1$ on the zero-field $C_p(T)$ curve coincides with the appearance of weak ferromagnetic response on the $\chi(T)$ curves measured at the low magnetic field (0.1 kOe). Thus, the magnetic behavior of $SrFe_2(PO_4)_2$ at low temperatures and low magnetic fields can be explained by a weak ferromagnetism due to spin canting. The canting angle, $\gamma$, can be estimated from the $M_0$ values using the simple equation, $\sin \gamma = M_0/gS\mu_B$.[25] At 2 K with $M_0 = 0.186\ \mu_B$/Fe-mol, $S = 2$, and $g = 2$, we obtain $\gamma \approx 2.7°$.

The Néel temperature ($T_N$) where the canted antiferromagnetism appears is therefore 7.0 K ($=T_1$) at zero magnetic field. For a conventional antiferromagnet, $T_N$ decreases with increasing magnetic field.[26] However, in $SrFe_2(PO_4)_2$, we observed unusual behavior when the first peak on the specific heat data corresponding to $T_N$ increases with increasing magnetic field (Figure 6b).

The position and intensity of the peak at $T_2$ on the $C_p(T)$ curves is independent of magnetic field below and at 15 kOe. No anomaly was also observed on the $\chi(T)$ curves near $T_2$ (11.3 K). These data give a strong support that the phase transition at $T_2$ in zero and small magnetic fields is not a magnetic phase transition but most probably a structural phase transition.

The temperatures of the structural phase transition ($T_2 = 11.3$ K) and magnetic phase transition ($T_1 = 7.0$ K) are close to each other in zero magnetic field. The temperature of the magnetic phase transition rises with increasing magnetic field. Thus, from a certain magnetic field (between 15 and 30 kOe), when the two peaks on the $C_p/T$ vs $T$ curves overlapped severely, we have observed the competition between the magnetic and structural phase transitions that was revealed by the appearance of the peak at $T_3 = 12.3$ K on the $C_p/T$ vs $T$ curves (Figure 6b). However the peak at $T_3$ on the $C_p/T$ vs $T$ curves has a magnetic origin because at the same temperature the peaks on the $d(\chi T)/dT$ vs $T$ curves were observed at 30 and 50 kOe (Figure 8b). The interesting question is whether the structural phase transition at $T_2$ persists at high magnetic fields or not. On the $C_p(T)$ curves, no clear peaks were observed at $T_2$ above 30 kOe.

The sigmoidal forms of the $M$ vs $H$ curves and anomalies on the $dM/dH$ vs $H$ curves at 2−11 K (Figures 9 and 11) indicates a metamagnetism probably due to the spin flip.[26−28] The small hysteresis found between 10 and 50 kOe at 5 and 6 K and between 5 and 20 kOe at 8 K is typical for soft ferromagnets. We can propose that the canted antiferromagnetic ground state below $T_1$ switches to another canted antiferromagnetic state with different spin direction above about 10−12 kOe. If we extrapolate magnetization between 30 and 50 kOe back to zero field, we obtain the induced ferromagnetic moment, $M_I$.[29] These values are listed in Table 4. A noticeable induced magnetic moment was observed even at 11 K, i.e., above $T_1$.

The hysteresis loop at 2 K showed well-defined magnetization jumps near $H = 0$ Oe (Figure 11). The $dM/dH$ vs $H$ curves at 5 and 6 K (Figure 9b) also indicated the presence of such jumps near $H = 0$ Oe. Similar jumps have been observed in other antiferromagnets that have a small net moment.[25] The jumps were suggested to be caused by abrupt changes in the domain structure, e.g., abrupt domain-wall motion.[25]

We can propose the following scenario to explain the complicated magnetic behavior of $SrFe_2(PO_4)_2$. The magnetic ground state is an antiferromagnetic one with spin canting. Application of magnetic field induces a spin flip to another spin-canted antiferromagnetic ordered state with different spin direction and larger net magnetic moment. This is the origin of metamagnetism. The spin direction of the ordered state is closely related to the crystal structure. The spin structure (spin direction) in the magnetic field is favored in the high-temperature (above $T_2$) structure. Therefore no structural transition is observed when $C_p$ is measured in high magnetic fields. The question arising is why $T_N$ increases with increasing magnetic field. The answer can be found in the structural features of this compound. As discussed above, $SrFe_2(PO_4)_2$ comprises Fe2−Fe1−Fe1−Fe2 spin clusters. Because of the intercluster interaction, the system gets ordered antiferromagnetically, but there should be a competition between the singlet state with a spin gap which is expected for a four-spin cluster and the long-range ordered state. In such a situation, $T_N$ increases with increasing magnetic field because the singlet state is unstable in a magnetic field. This scenario is just a speculation at this stage of the research. Detailed neutron diffraction experiments in magnetic fields are required to clarify the mechanisms of magnetic phase transitions.

The domination of the long-range ordering can be explained by the geometry of the Fe−O−Fe connections. The Fe1−O−Fe2 bond angles in the four-spin cluster are close to 90° or ever smaller than 90° (Figure 4). The Fe1−O4−Fe1 bond angles are far from 180°, which is most favorable for a large antiferromagnetic exchange constant. The Fe1−O1−Fe2 connections between the clusters include the long Fe2−O1 distance. Thus, exchange constants between Fe atoms mediated by O atoms should be small. On the other hand, it is known that relatively large exchange interactions between magnetic ions can be provided by $PO_4$ groups.[30] Thus, the $PO_4$ groups seem to be responsible for the three-dimensional connections between Fe atoms in $SrFe_2(PO_4)_2$.

(25) Adams, R. D.; Layland, R.; Payen, C.; Datta, T. *Inorg. Chem*. **1996**, *35*, 3492.
(26) Carlin, R. L. *Magnetochemistry*; Springer-Verlag: Berlin, 1986; 327 pp.
(27) Zheng, L.-M.; Gao, S.; Song, H.-H.; Decurtins, S.; Jacobson, A. J.; Xin, X.-Q. *Chem. Mater*. **2002**, *14*, 3143.
(28) Yin, P.; Gao, S.; Zheng, L.-M.; Wang, Z.; Xin, X.-Q. *Chem. Commun*. **2003**, 1076.
(29) Herweijer, A.; de Jonge, W. J. M.; Botterman, A. C.; Bongaarts, A. L. M.; Cowen, J. A. *Phys. Rev. B* **1972**, *5*, 4618.
(30) Belik, A. A.; Azuma, M.; Takano, M. *Inorg. Chem*. **2003**, *42*, 8572.

The magnetic phase diagrams of antiferromagnets showing metamagnetism and spin−flop transitions (e.g., for $FeCl_2$, $FeBr_2$, and $CoCl_2$)[31,32] have attracted appreciable interest in recent years. In this work, we have shown that $SrFe_2(PO_4)_2$ has interesting and unusual magnetic properties including metamagnetic regimes and competition between structural and magnetic phase transitions. The more thorough investigation of magnetic anisotropy using single crystals is desirable to study all details of magnetic phase diagram for $SrFe_2(PO_4)_2$.

In conclusion, we have successfully determined the structure of $SrFe_2(PO_4)_2$ from laboratory XRD data. $SrFe_2(PO_4)_2$ presents a new structure type among $AB_2(XO_4)_2$. We have investigated magnetic properties of $SrFe_2(PO_4)_2$ and showed it to be a canted antiferromagnet below 7.0 K. The presence of several phase transitions induced by magnetic field was confirmed by the specific heat and dc magnetization measurements.

**Acknowledgment.** The authors express their thanks to the Ministry of Education, Culture, Sports, Science and Technology, Japan, for Grants-in-Aid No. 12CE2005, for COE Research on Elements Science (No. 13440111 and No. 14204070), and for 21COE on the Kyoto Alliance for Chemistry.

**Supporting Information Available:** FC $\chi T$ vs $T$ curves at 0.1, 5, 15, 30, 50, and 90 kOe in the temperature range of 2−27 K (Figure S1), $M$ vs $H$ curves at 5, 6, and 8 K emphasizing the second hysteresis and the first magnetization curves at 2, 5, 6, and 8 K (Figure S2), $M$ vs $H$ and d$M$/d$H$ vs $H$ curves at 9, 10, 11, and 13 K (Figure S3), and real ($\chi'(T)$) and imaginary ($\chi''(T)$) parts of the alternating current susceptibility at zero static magnetic field (Figure S4) (PDF). This material is available free of charge via the Internet at http://pubs.acs.org.

CM049140O

(31) Suzuki, I. S.; Huang, T.-Y.; Suzuki, M. *Phys. Rev. B* **2002**, *65*, 224432.
(32) Aruga Katori, H.; Katsumata, K.; Petracic, O.; Kleemann, W.; Kato, T.; Binek, Ch. *Phys. Rev. B* **2001**, *63*, 132408.